PROTEINS: Structure, Function, and Genetics 43:175–185 (2001)

Structural Basis for Altered Activity of M- and H-Isozyme Forms of Human Lactate Dehydrogenase

J.A. Read, V.J. Winter, C.M. Eszes, R.B. Sessions, and R.L. Brady*
Department of Biochemistry, University of Bristol, Bristol, United Kingdom

ABSTRACT **Lactate dehydrogenase (LDH) interconverts pyruvate and lactate with concomitant interconversion of NADH and NAD^+. Although crystal structures of a variety of LDH have previously been described, a notable absence has been any of the three known human forms of this glycolytic enzyme. We have now determined the crystal structures of two isoforms of human LDH—the M form, predominantly found in muscle; and the H form, found mainly in cardiac muscle. Both structures have been crystallized as ternary complexes in the presence of the NADH cofactor and oxamate, a substrate-like inhibitor. Although each of these isoforms has different kinetic properties, the domain structure, subunit association, and active-site regions are indistinguishable between the two structures. The pK_a that governs the K_M for pyruvate for the two isozymes is found to differ by about 0.94 pH units, consistent with variation in pK_a of the active-site histidine. The close similarity of these crystal structures suggests the distinctive activity of these enzyme isoforms is likely to result directly from variation of charged surface residues peripheral to the active site, a hypothesis supported by electrostatic calculations based on each structure. Proteins 2001;43:175–185.** © 2001 Wiley-Liss, Inc.

Key words: oxidoreductase; crystal structures; isoforms; electrostatic surface charges; kinetics

INTRODUCTION

One consequence from emerging genomic data is the frequent occurrence of multiple, homologous forms of near-identical enzymes in the same organism. Termed isozymes, these enzymes are derived from individual genes, which are translated to proteins with similar sequences and activities, but each with distinctive kinetic or regulatory properties. One of the earliest examples of isozymes, and that which is still most frequently quoted in elementary biochemistry textbooks, is provided by the essential glycolytic enzymes of the L-lactate dehydrogenase family.[1]

L-Lactate dehydrogenases (LDH) are a family of 2-hydroxy acid oxidoreductases that simultaneously and stereospecifically interconvert pyruvate to lactate, and NADH to NAD^+:

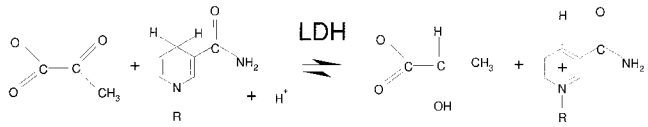

This reaction, known as anaerobic homolactic fermentation, forms an important means of regenerating NAD^+, enabling the continuation of glycolysis. Most mammals express several isozymes of LDH. The two major forms of LDH found in *Homo sapiens* are the M form (M_4-hLDH), found predominantly in anaerobic tissues such as skeletal muscle and liver (corresponding to the human A gene), and the H form (H_4-hLDH) which predominates in mainly aerobic tissues such as cardiac muscle (corresponding to the human B gene). A third type has also been identified, the X form, which appears to be restricted to the testes. Amino acid sequence identity between the M and H forms is high (75%; Table I), but there are significant differences in the reported kinetic properties of each form (Table II). At pH 6.0, for example, the M_4 species displays a K_M for pyruvate around 3–10-fold higher than measured for the H_4 form. As the different subunits can combine to form mixed or hybrid tetramers (H_4, MH_3, M_2H_2, M_3H, and M_4), it seems likely that their structures are also highly conserved.[2] Both forms also share considerable similarity with pig LDH isoforms (97% and 92% sequence identity between H and M forms respectively). These are the closest homologues for which crystal structures are known.

Structural analyses of LDH from a range of species are well advanced and include crystal structures of these enzymes from dogfish,[3] pig,[4,5] *Bacillus stearothermophilus*,[6] *Bifidobacterium longum*,,[7] and *Plasmodium falciparum*.[8] Despite considerable amino acid sequence diversity between each of these proteins, a high level of structural similarity is preserved. These enzymes usually form tetramers with 222 symmetry, with each of the four 330 amino acid subunits forming a bilobal structure of two

Grant sponsor: Biotechnology and Biological Sciences Research Council (BBSRC).

*Correspondence to: R.L. Brady, Department of Biochemistry, University of Bristol, Bristol BS8 1TD U.K. E-mail: L.Brady@bris.ac.uk

Received 8 August 2000; Accepted 8 December 2000

TABLE I. Percentage Amino Acid Sequence Identity Among H, M, and X Forms of Selected Mammalian LDH

	H Form			M Form			X Form
	Human	Pig	Mouse	Human	Pig	Mouse	Human
Pig H	97	—	—	—	—	—	—
Mouse H	97	95	—	—	—	—	—
Human M	75	74	74	—	—	—	—
Pig M	76	75	75	92	—	—	—
Mouse M	75	75	75	93	93	—	—
Human X	69	68	68	74	75	74	—
Mouse X	63	63	72	72	71	72	73

LDH, lactate dehydrogenase.

TABLE II. Reported Kinetic Parameters for H and M Forms of Human and Pig LDH†

	Human		Pig	
	H_4-LDH	M_4-LDH	H_4-LDH	M_4-LDH
Steady-state k_{cat} (s^{-1})	143[12]	260[11]	200[26]	450[30]
K_M pyruvate (mM)	0.058[12]	0.158[11]	0.095[27]	0.6[30]
K_i pyruvate (mM)	0.77[12]	3.9[11]	—	—
K_d NADH (μM)	0.53[12]	0.62[11]	0.51[28]	3.7[28]
K_d NAD^+ (μM)	165[12]	198[11]	300[28]	500[28]
K_d oxamate (mM)	0.0087[12]	0.026[11]	0.027[29]	0.15[30]

LDH, lactate dehydrogenase.
†Conditions of measurement used in references (superscript numbers) 11 and 12 were pH 6.0, 25°C, 20 mM Bis–Tris and 50 mM KCl; reference 26: pH 6.0–7.8, 20°C, 50 mM phosphate, 100 mM NaCl; reference 27: pH 8.0, 20°C, 100 mM phosphate; reference 28: pH 7.2, 20°C, 67 mM phosphate; reference 29: pH 7.0, 21°C, 100 mM phosphate; reference 30: pH 7.5, 23°C, 100 mM phosphate.

domains. The larger domain adopts an archetypal "Rossmann" fold and provides the NADH-cofactor binding site. Adjacent to the nicotinamide group of the cofactor, the pyruvate/lactate binding pocket is formed at the interface with the adjoining mixed α/β "substrate-binding" domain. Binding of cofactor is followed by substrate in an ordered catalytic process (reviewed in ref. 5) and includes enclosure of the active site through ordering of an "active-site loop" (residues 99–110) from which an invariant arginine (109) is believed to stabilize the transition state in the hydride-transfer reaction. Contacts between residues 101–103 from this loop and the substrate are the main determinant of enzyme specificity,[9] a system also shared by the related, but dimeric, malate dehydrogenases.[10] This model for enzyme activation and specificity has been derived from comparisons of a variety of dehydrogenase crystal structures in apo, binary, and inhibitory ternary complex forms, and extensive mutagenesis and kinetic analyses.[2]

A surprising absence from this composite picture derived from lactate dehydrogenase structures is any structure of the three known isozymes of human LDH. Although the high level of sequence identity supports the use of the pig structures as good models for human LDH function, attempts to target LDH for specific inhibitor (drug) design (e.g., against *Plasmodium* LDH[8]) require a more precise understanding of human LDH structures. In addition, although crystal structures exist for both H and M forms of pig LDH, the differing resolutions and qualities of these structures complicate an accurate comparison of these two isozymes. In this article, we describe both the determination of the crystal structures of the major isoforms of human LDH (M and H), and the use of these data to probe the structural basis of the individual activities of these isozymes. The structures have been refined to 2.3- and 2.1-Å resolution (M and H, respectively), enabling us to examine the two active sites in detail. We have also measured the effect of pH on the activity of each isozyme, and correlate these results with the crystal structures. Calculations of electrostatic potentials from each structure suggest that the unique activity of each form of human LDH arises from the variation of surface residues peripheral to the active site, which itself is strictly preserved. These data illustrate a simple method of evolving modified enzyme activity in this family of enzymes.

MATERIALS AND METHODS

Expression, Purification, and Crystallization of M_4-hLDH and H_4-hLDH

Recombinant human M_4-hLDH and H_4-hLDH were expressed in *Escherichia coli* cells using the vector p*KK*223-3 (Pharmacia) as previously described.[11,12] Both fully activated proteins were purified in a single step by affinity chromatography on an oxamate agarose column in the presence of NADH as previously described.[13]

Crystals of both forms of hLDH were grown by hanging drop vapor diffusion at 18°C. Crystals of M_4-hLDH were

TABLE III. Summary of Data Collection and Refinement Statistics for the Crystal Structures of M_4-hLDH and H_4-hLDH

	M_4-hLDH	H_4-hLDH
Resolution range (Å)	30–2.3 (2.4–2.3)	30–2.1 (2.2–2.1)
R_{merge}	8.1 (19.5)	11.4 (5.0)
Redundancy	3.5 (3.5)	3.3 (3.1)
Completeness	92.3 (89.0)	96.0 (91.1)
$\langle I \rangle / \langle \sigma I \rangle$	14.1 (5.4)	21.2 (8.5)
No. of unique reflections	112344	37680
No. of reflections used in refinement	105,726	35,493
No. of reflections in free R set	5,564	1,867
No. of atoms refined (protein + NAD)	21,790	5,204
No. of waters	757	218
R-factor (all data in the resolution range)	20.9	19.5
R-free (all data in the resolution range)	27.1	24.4
Average B_{iso} for protein atoms (Å^2)	24.3	19.7
Average B_{iso} for waters (Å^2)	23.2	22.4
Overall B_{iso} (Å^2)	24.3	19.9
RMSD for bond length (Å)	0.012	0.013
RMSD for angle (degrees)	1.75	1.76

LDH, lactate dehydrogenase; RMSD, root-mean-square deviation.

obtained by mixing equal volumes of a well solution containing 12% PEG 8000 (Fluka), 100 mM sodium acetate in 100 mM sodium HEPES pH 7.5, with a protein solution comprising 28 mg/ml M_4-hLDH, 2.5 mM NADH and 1 mM sodium oxamate 100 mM HEPES at pH 7.5. Crystals were large, thick rectangular plates of approximate dimensions 100 μm × 300 μm × 500 μm.

Crystals of H_4-hLDH were obtained under similar conditions. The well solution contained 21% PEG 8000 (Fluka), 100 mM sodium acetate in 100 mM Sodium HEPES pH 7.5, and protein solution comprising 15 mg/ml H_4-hLDH, 2.5 mM NADH and 1 mM sodium oxamate in 50 mM HEPES at pH 7.5. Crystals were small, cracked rods of approximate dimensions 30 μm × 50 μm × 100 μm.

Data Collection

Crystals of M_4-hLDH were cryopreserved in a solution which contained 17% PEG 8000, 100 mM sodium acetate, and 20% glycerol. An initial data set to 2.8 Å resolution was collected at the EMBL (Hamburg) beamline X11 at 100 K. The crystals produced were orthorhombic with cell dimensions of $a \sim 65$ Å, $b \sim 160$ Å, $c \sim 265$ Å. The data extended to ~2.0 Å, but it was not possible to process data to a resolution of >2.8 Å due to the high mosaicity (~1°) of the crystals. Improvement in the flash cooling conditions, requiring 1% incremental increases in the concentration of PEG 8000 and that of glycerol by 5% over 2 min, permitted data that extended to 2.3-Å resolution to be collected at Daresbury SRS, station PX7.2 (wavelength = 1.488) on a Mar 345-mm image plate. The crystal had a mosaicity of ~0.25°. The oscillation angle for data collection was reduced to 0.5°. The data were processed using DENZO and scaled with SCALEPACK.[14] Crystals were of $P2_12_12_1$ symmetry, with $a = 64.9$ Å, $b = 158.5$ Å $c = 266.2$ Å. There are two M_4-hLDH tetramers in the asymmetric unit. Data collection statistics are summarized in Table III.

Crystals of H_4-hLDH were flash cooled to 100 K in a solution containing 25% PEG 8000, 100 mM sodium acetate and 10% glycerol. Data to 2.1-Å resolution were collected at Daresbury SRS, station PX7.2 (wavelength = 1.488) on a Mar 345-mm image plate. The data were processed using DENZO and scaled with SCALEPACK.[14] Crystals were of $C222_1$ symmetry, with $a = 59.5$ Å, $b = 161.7$ Å, $c = 137.8$ Å. There are two H-hLDH monomers in the asymmetric unit. Data collection statistics are also summarized in Table III.

Structure Determination

The structure of M_4-hLDH at 2.3 Å was solved by molecular replacement with AMORE.[15] The coordinates of a tetramer of porcine muscle LDH[5] (PDB 9ldt) solved at 2.0 Å were used as a search model. Two unique solutions were found, representing the two independent tetramers of M_4-hLDH in the asymmetric unit. The molecular model was improved by cycles of manual rebuilding, using O,[16] and crystallographic refinement with REFMAC.[17] Each subunit was treated independently throughout the refinement, as the implementation of noncrystallographic symmetry proved deleterious to the free R factor. Water molecules were added using ARPP[18] and checked manually. The final refinement statistics are summarized in Table III.

The structure of H_4-hLDH at 2.1 Å was solved by molecular replacement with AMORE.[15] The coordinates of porcine heart LDH[4] (5ldh) solved at 2.7 Å were used as a search model. A single solution was found. The molecular model was improved by cycles of manual rebuilding, using O,[16] and crystallographic refinement with REFMAC.[17] Water molecules were added using ARPP[18] and checked manually. The final refinement statistics are shown in Table III.

Kinetic Measurements

Initial rates of decrease in NADH concentration were monitored at 340 nm (366 nm for pyruvate concentrations of >50 mM) at 25°C. The buffers used were: at pH 5.5: 20 mM MES with 50 mM KCl; at pH 6.0, 6.5, and 7.0: 20 mM Bis-Tris with 50 mM KCl; at pH 7.5, 8.0, 8.5, and 9.0: 20

mM Tris with 50 mM KCl; at pH 9.5: 20 mM CHES with 50 mM KCl. Catalysis was initiated by the addition of protein. Data were fitted to the Michaelis–Menten equation (corrected for substrate inhibition) using the following equation and the nonlinear regression facility in Grafit 3.0[19]:

$$V/V_{max} = S/[S + K_M + (S^2/K_i)]$$

where S is the substrate concentration and V is the velocity at substrate concentration S. The coenzyme concentration was 0.2 mM for both enzymes, and pyruvate concentration ranges were 10 μM–0.1 M in each case. The protein concentration used was 10 nM. Calculations of k_{cat} depended on the protein concentration as measured at 280 nm using an extinction coefficient of 1.16 mg/mL · cm for H_4-hLDH and 1.2 mg/mL · cm for M_4-hLDH. The K_M values were plotted against pH (see Fig. 5) and the data fitted with Grafit to the equation:

$$K_{M(obs)} = K_M[1 + 10^{-pK}/10^{-pH}]$$

Electrostatic Potential Calculations

Electrostatic potential calculations were performed using DelPhi (MSI). This program is an implementation of the linearized Poisson–Boltzmann model developed by Gilson and Honig[20] and treats the solvent and protein as different continuum dielectric media. The most efficient way to calculate the effect of a charged residue R in the protein upon the pK_a of the active-site histidine is to place a unit charge on atom NE2 of His 195, and calculate the electrostatic potential at the position of the charged group of residue R. This effect will be identical to the electrostatic potential at His 195 caused by placing a charge at residue R.

A set of residues was defined corresponding to all those charged residues that result in a change in charge between the H and M isoforms. This corresponds to 14 residues in the M isoform and 13 in the H isoform. Summing the calculated potentials over these residues gives the shift in pK_a for His 195 between the two isoenzymes. In these calculations, all four subunits of the tetramer were included and the calculated potentials averaged over each equivalent residue position. The electrostatic potentials were measured at CZ in Arg, NZ in Lys, and averaged over OD1 and OD2 in Asp and OE1 and OE2 in Glu residue types. The calculations were first performed on a coarse grid (M: 51 × 65 × 67, spacing 2.104 Å; H: 57 × 65 × 65, spacing 2.104 Å) surrounding the whole tetramer plus a 20 Å border region. Two subsequent focusing calculations were performed for each residue in the set, with grid geometries (65 × 65 × 65, spacing 0.6250 Å) and (65 × 65 × 65, spacing 0.3125 Å). These focusing grids were centered on the atom adjacent to the charged group in each case (CG for Asp, CD for Glu, NE for Arg and CE for Lys). In all calculations, the following parameters were used: dielectric constants of 2.0 and 78.5 for the protein interior and solvent respectively; a 2.0 Å Stern layer and a 1.4 Å probe radius; an ionic strength of 0.07 M.

Three protein models based on the crystal structures of each isoform were used in the calculations. Model TERN consisted of the crystal structures of protein, NADH and oxamate. Model BIN had the oxamate removed and the active-site loop conformations (M: G99-L100; H: G99-L100) randomized by molecular dynamics. Model XLOOP had the oxamate removed and the active-site loops removed (M: A100-R109; H: V100-R109). In each case, all crystallographic waters were removed with the intention of making the models directly comparable. The results of the calculations are presented in Table V, where potential values in units of kT have been converted into Δ pK_a by dividing by 2.303. The randomization of the active-site loop conformation was performed by first removing oxamate and crystallographic waters and adding hydrogen atoms to both M and H tetramers such that any possibly charged residues were neutral. All protein residues were then fixed in their crystallographic positions, with the exception of the active-site loop residues (M: G99-L100; H: G99-L100). The loops were subjected to 10-ps molecular dynamics at 1500 K, annealed for 5 ps at 300 K and relaxed with 200 cycles of conjugated gradient minimization (see Fig. 7).

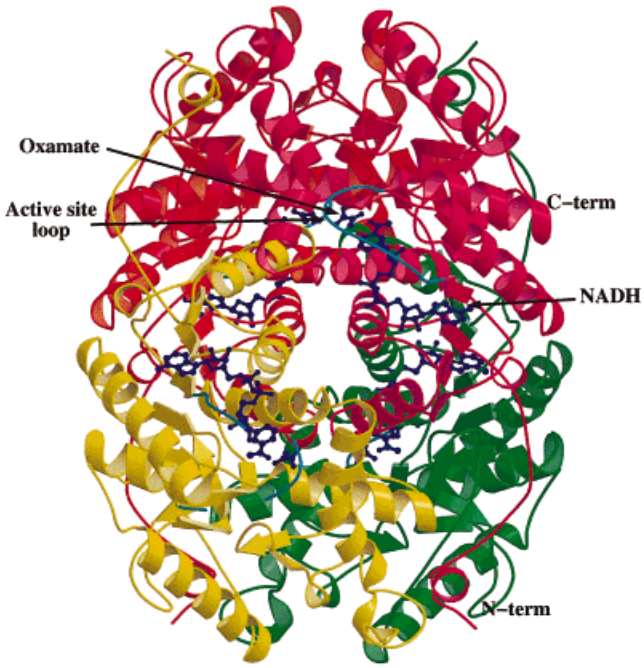

Fig. 1. Tetrameric structure of hLDH. MOLSCRIPT traces showing a tetramer of H_4-hLDH. The NADH cofactor and oxamate substrate analogue are shown in ball-and-stick representation in blue, and the active-site loop is highlighted in cyan. The individual subunits are colored differently, and the amino- and carboxy-termini of the red subunit are labeled N-term and C-term, respectively.

RESULTS AND DISCUSSION

Overall Structure

In both structures, human LDH is seen to assemble to a tetramer with 222 symmetry (Fig. 1). Each monomer displays the familiar LDH fold. There are two domains: the larger with a "Rossmann"-type fold formed by residues 20–162 and 248–266, and the accompanying mixed α/β

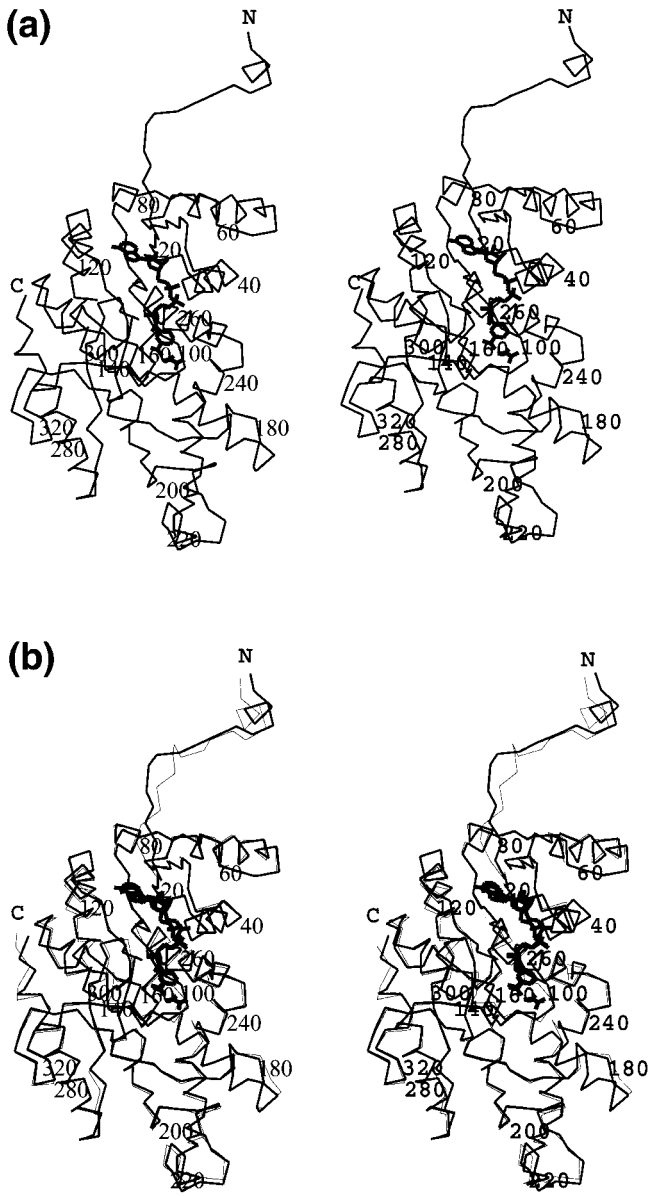

Fig. 2. Subunit structure of hLDH. Stereo Cα trace showing (**a**) a subunit of M_4-hLDH, and (**b**) a subunit of H_4-hLDH (thin lines) overlaid on the M_4-hLDH subunit (thick lines). In each case every 20th residue is labeled, and the amino- and carboxy-termini are labeled, N and C, respectively. The NADH cofactor and oxamate substrate analogue are shown in bold.

"substrate binding" domain comprising residues 163–247 and 267–331. This latter domain consists of four β-strands and three helices, whereas the larger domain has a central, 6-stranded parallel β-sheet flanked by three helices on each side (Fig. 2). The cofactor binds in a groove at one end of the central β-sheet, with residues His 195, Asp 168, Arg 171, and Thr 246 all making major contributions to the catalytic geometry in the active site. In these ternary complexes the "active-site loop" residues 99–110 enclose the active site, with Arg 109 hydrogen bonded to the carbonyl of the substrate. The substrate-binding cavity is located at the interface of the two domains. The first 20 residues at the N-terminus adopt an extended conformation and wrap around the adjacent subunit in the tetramer. All these features have previously been described in the structures of other mammalian LDH.[2]

In crystals of M_4-hLDH, there are two tetramers forming the asymmetric unit, whereas there is only a single dimer in the asymmetric unit of the H form, where the tetramer is generated by the crystallographic symmetry. The M-form crystals therefore contain 8 independent monomers of M-hLDH, all of which have been treated independently during refinement. An overlay of four of the M-hLDH monomers (Fig. 3a) shows the considerable overall structural integrity of the fold. Root-mean-square deviations (RMSD) of all 331 equivalent Cα positions between each of the four subunits are within the range 0.3–0.5 Å. There are, however, several regions in which limited variations are seen. The largest displacements between the structures are seen in the N-terminal 20 amino acids (typical equivalent Cα displacement: 3 Å), which are in an extended conformation and wrap around the adjacent subunit. Similar variations are seen in a second region, the 99–110 active-site loop. Ordering of this loop is accompanied by substrate binding as in other LDH structures. In hLDH, small changes in conformation reflect local crystal contacts in the tetramer. A third region of notable variation occurs in the location of the neighboring C-terminal helix (α-H). Here the positions of equivalent Cα atoms vary typically by up to 1.6 Å, a significant change indicating overall displacement of this secondary structure element. Movement of this helix, which forms hydrogen bonds with groups at the base of the active-site loop, has previously been observed in transitions between binary and ternary complexes of pig LDH within the same crystal lattice.[5] Mutagenesis of residues forming these connective hydrogen bonds is known to affect the turnover rate of a closely related enzyme, malate dehydrogenase.[21] The relative mobility of this unit observed in the comparison of eight subunits of M-hLDH is consistent with movement of this region during catalysis.

The two independent copies of H-hLDH found in the crystallographic asymmetric unit also show overall close similarity (RMSD of 330 equivalent Cα positions: 0.90 Å), with variations restricted to similar regions (Fig. 3b). Again, the 20 N-terminal residues in an extended conformation are displaced by ≤3 Å between the two separate subunits. Residues in the active-site loop in this crystal form are highly conserved in their positioning, whereas displacement of the C-terminal helix α-H is more pronounced. Here equivalent Cα positions are displaced by an average of about 2 Å. One further region of significant flexibility is seen in the 220–226-loop region. Located on the exterior surface of the tetramer and about 25 Å distant from the active-site cavity, this loop has previously been noted as a source of antigenic variation between forms of LDH and has been termed the "antigenic loop."[22]

M_4-hLDH- and H_4-hLDH differ in 81 out of 331/332 amino acid positions, but this is seen to generate negligible differences in the overall structures where monomers from each form overlay with a RMSD of 0.82 Å (300 equivalent

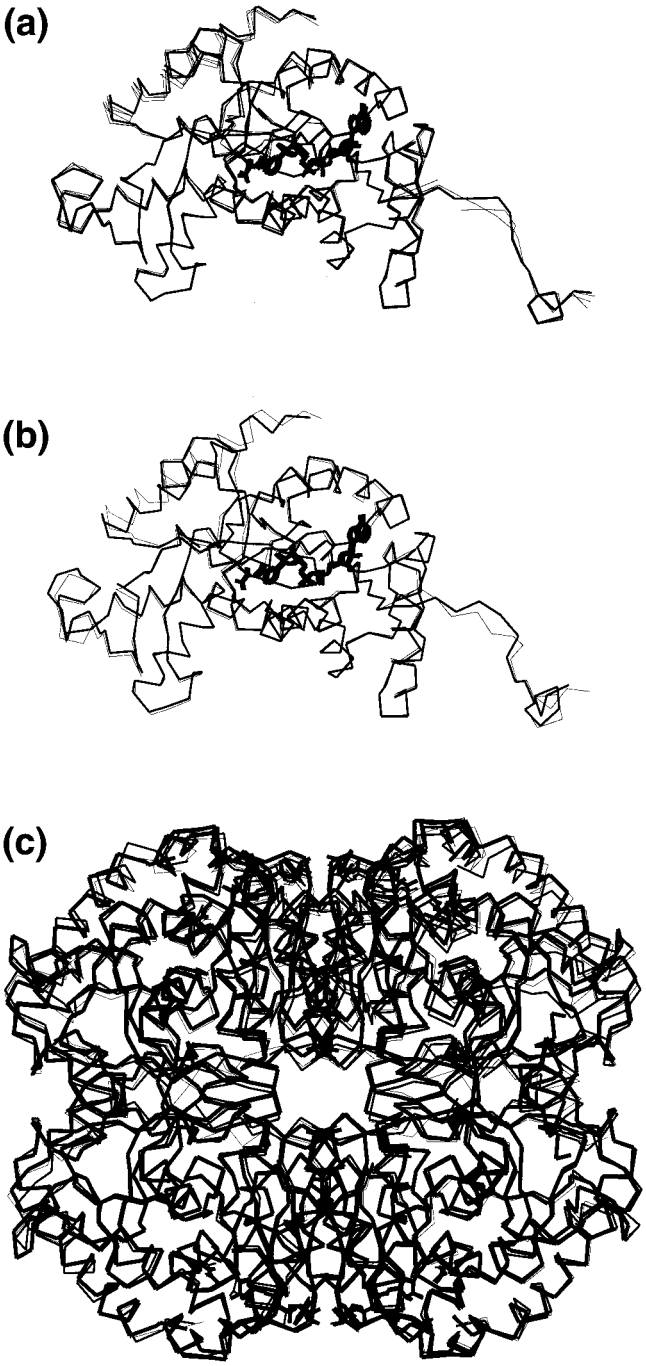

Fig. 3. Subunit variation in hLDH. **a:** Overlay of Cα traces for four of the independent monomers of M-hLDH in the asymmetric unit. **b:** Overlay of Cα traces for both of the independent monomers of H-hLDH in the asymmetric unit. **c:** Overlay of Cα traces for each of the two independent tetramers of M_4-hLDH (thin and medium lines) on the tetramer of H_4-hLDH (thick lines). In each case, the fit has been maximized for a single subunit of the tetramer (lower right in this view).

Cα positions in subunits A; Fig. 2b). Again, significant structural variations are restricted to the regions already noted for each form of hLDH. This overlay of all independent copies of hLDH from both structures indicates those regions of the molecules that are inherently flexible and

TABLE IV. RMSD of Various Mammalian LDH Crystal Structures

Species (d_{min} of crystal structure)	RMSD (Å)	No. of Cα positions compared
Human H (2.1 Å): human M (2.3 Å)	0.79	330
Human H (2.1 Å): pig H (2.7 Å)	2.42	330
Human M (2.3 Å): pig M (2.2 Å)	0.56	330
Human H (2.1 Å): mouse X (3.0 Å)	1.03	294
Human M (2.3 Å): mouse X (3.0 Å)	1.00	294
Pig H (2.7 Å): pig M (2.2 Å)	1.72	314
Pig H (2.7 Å): mouse X (3.0 Å)	2.00	294
Pig M (2.2 Å): mouse X (3.0 Å)	0.98	294

RMSD, root-mean-square deviation; LDH, lactate dehydrogenase.

partially illustrates the effective experimental "error" derived from the different crystallographic lattices and refinement. Mobility of the α-H C-terminal helix is particularly prominent in this comparison.

A similar pattern is repeated when individual subunits of hLDH are compared with monomers of LDH from other species. Table IV shows the RMSD of equivalent Cα positions from the two human LDH structures as compared with the pig H, pig M, and mouse X LDH structures. Table IV also shows the reported resolution of each crystal structure, to give some indication of the precision of each model. One notable feature is the significantly enhanced differences reflected in the RMS values for all comparisons involving the pig H_4-LDH structure. These differences would not be expected from the comparison of the amino acid sequences (Table I) that do not indicate pig H_4-LDH as an outlier as the structural comparison suggests. Published in 1980, this crystal structure considerably predates all the other LDH structures used in this comparison. Structure determination methods have improved considerably since that time, so it seems likely that the later, higher-resolution structures present more accurate representations. Structural comparisons of LDH isoforms from the same species have previously been restricted to the pig H and M forms, this suggests the current structures of human H and M forms, determined to similar resolutions, present a better opportunity to accurately compare differences between isoforms. The significant variations between the human and pig H-form structures also emphasize the limitations of using the pig LDH structure as a mimic for human LDH in drug-design studies. The absence of significant structural differences between the conformations of the monomers of the human isoforms fails to provide an explanation for the differences in their kinetic behavior.

Variations in Assembly

Comparisons of pig H- and M-form LDH tetramer structures suggest that each homotetramer is distinguished by small variations in mode of assembly. The human isoform structures are of comparable resolution and allow us to reassess the significance of these variations. The small changes in the N-terminal region referred to above reflect a slight but significant alteration in the

subunit associations between the tetramers of H- and M-form hLDH. Figure 3c shows a comparison of the two independent tetramers from the asymmetric unit of M_4-hLDH with the tetramer of H_4-hLDH. In each case the fit has been restricted to a single subunit. It can be seen that the remaining monomers appear to be slightly displaced, reflecting a small change in the relative associations of the subunits between the structures. This displacement in the diametrically opposed domain equates to an average translational displacement of 0.7 Å and a rotation of 0.8° for all Cα atoms. These small changes are likely to be of marginal significance, given the resolution of these structures. Nonetheless, these average displacements calculated across all residues do not portray the larger changes at the periphery of each domain, where significant displacements of 1.4 Å and rotations of ≤5° are observed. However, because similar displacements are observed between each of the M-form tetramers, as well as when H- and M-form tetramers are compared, it seems unlikely that these changes have biological significance. This is supported by many early studies noting the ability of different isoforms of LDH to form mixed tetramers (H_1M_3, H_2M_2, H_3M_1), which is only likely to be feasible if the interfaces between subunits are largely conserved.

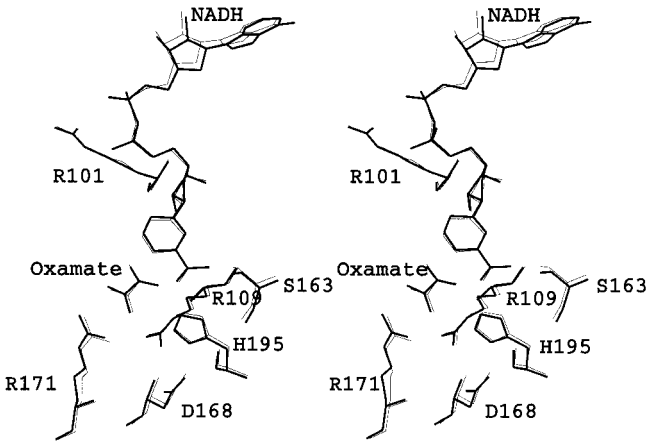

Fig. 4. Active site of hLDH. Overlay of key amino acids constituting the active site of M_4-hLDH (thin lines) and H_4-hLDH (thick lines). The NADH cofactor and oxamate substrate analogue are also shown for each structure.

Structure–Function Relationships

The predominance of M-type LDH in mainly anaerobic tissues, and H-type in LDH in aerobic, cardiac tissue, implies the adaptation of each for different redox environments.[1] Any such adaptations might be expected to be manifest in a comparison of their respective structures. Lactate dehydrogenases have been the subject of extensive kinetic analyses.[2] Table II summarizes the kinetic data derived from a number of sources for the H and M forms of both human and pig LDH and includes data measured for the two recombinant forms of hLDH used in this study. These data show small but consistent differences in the kinetic constants between H and M forms of each enzyme. In each case, the overall turnover rate is increased by an approximate factor of 2 for the M over the H form. The K_d values for both NADH and NAD^+ for the two human isoforms remain relatively constant, with the increase in activity being related almost entirely to a threefold enhancement in binding of the substrate pyruvate (or its analogue, oxamate) in the H-form of the enzyme.

Dunn et al.[5] summarized an extensive range of experiments from which many of the details of the catalytic mechanism of LDH have been derived. Catalysis is an ordered event, initially requiring binding of the nicotinamide cofactor. Binding of the charged substrate induces closure of the specificity loop, precluding solvent from access to the active site and hence facilitating hydride transfer. Loop closure is concomitant with small movements of the α-D helix at its base, and concerted movement of the C-terminal α-H helix. This is the helix with which small movements are associated when the different subunits of hLDH are compared. The roles of many active-site residues have been deduced from a combination of kinetic analysis of site-directed mutants and crystallographic analysis. In the presence of pyruvate, the protonated His 195 acts as the catalytic acid and is stabilized by Asp 168. Substrate recognition is provided by a cluster of residues, including Ala 236, Thr 246, Arg 171, Gln 102, and Arg 109. The latter two are located on the underside of the active-site loop and come into contact with the substrate upon loop closure. All of these, and the residues that form the cofactor binding pocket, are conserved in both identity and conformation between the two isoforms of hLDH (Fig. 4; RMSD for all atoms of the cofactor, substrate analogue, and amino acids R101, R109, S163, D168, R171, and H195 is 0.17 Å).

The strict preservation of the active-site features between the two isoforms, together with an absence of any obvious correlation with quaternary structural changes, led us to examine other features of the hLDH structures that might distinguish their activities. As the affinity for the cofactor remains constant between the two isoforms, we surmised that the differing kinetic properties of the isoforms are likely to arise from events related to substrate binding accompanied by closure of the active-site loop. The identity and conformation of residues on the underside of the specificity loop, and the residues against which they dock in the activated complex, remain constant between the H- and M-form structures. The small movements observed in the adjacent α-H helix do not distinguish each of the isoform structures, and as the interface between this region and the active-site loop is conserved, the involvement of this region seems unlikely.

Figure 5 plots the variation in pH of the experimentally determined K_M for pyruvate for both H and M forms of hLDH. In this reaction, it can be shown that K_M for pyruvate is an apparent K_d for pyruvate: representing $K_M = (k_{cat}+k_{off})/k_{on}$, taking k_{on} as diffusion controlled at $10^8\ M^{-1}\ s^{-1}$, $k_{cat} = 200\ s^{-1}$ and the limiting case of $K_M = 50\ \mu M$, shows that $k_{off} = 4800\ s^{-1}$; i.e., the Michaelis constant is dominated by the K_d component. This assumption is also empirically substantiated by the fact that the K_d for oxamate (a substrate analogue) tracks the K_M for

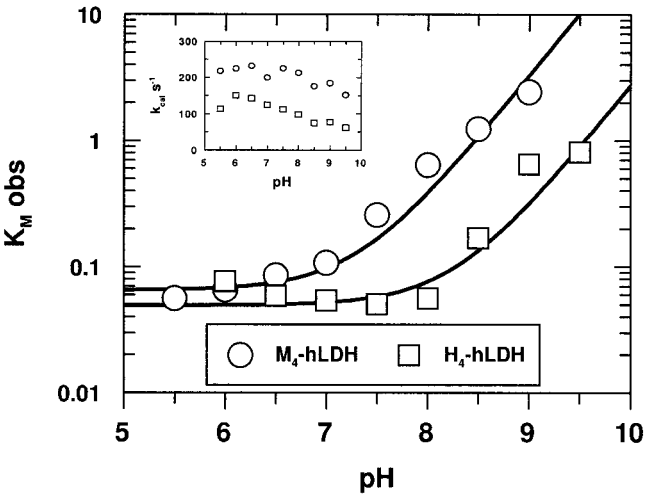

Fig. 5. Variation of pyruvate K_M with pH. The experimentally determined K_M values for pyruvate are plotted with H_4-hLDH (□) and M_4-hLDH (○) versus pH, and the corresponding fits. Inset, corresponding values of k_{cat} measured at each pH.

pyruvate in these LDH (Table II). Both isoforms have small values of K_M at low pH, consistent with pyruvate binding to an active site possessing a protonated catalytic histidine. Since pyruvate is unable to bind to the active site having an unprotonated histidine, the K_M for pyruvate rises as the pH rises above the pK_a of His 195. The data in Figure 5 fit to a model involving the ionization of a single group, giving pK_a values of 7.31 ± 0.11 and 8.26 ± 0.15 for the M and H forms, respectively, consistent with His 195. These apparent variations in the basicity of the catalytic group, despite the strong local conservation of its surrounding environment, led us to examine the possible influence of surface electrostatic charges upon the pK_a of His 195. The k_{cat} values for pyruvate with both isoenzymes do not vary by more than a factor of 2 over this pH range, and these data are shown in Figure 5 (inset).

Surface Charges Distinguish Isoforms of hLDH

Comparison of the amino acid composition of the two isoforms shows that H-hLDH has an overall net charge of −6, while the net charge of the M form is +1 (per subunit). It is difficult to evaluate the precise charge distribution in the region of the respective active sites as many of the charged surface residues are distorted through the many and varying contacts between subunits in the two crystal lattices. Figure 6 shows the location of all amino acid changes between H- and M-form hLDH in which the change in amino acid identity results in a net change in charge (i.e., uncharged to charged amino acid, and vice-versa; and positively charged to negatively charged). As might be expected, the majority of these changes cluster on solvent-exposed surfaces away from the tetramer interfaces. However, there is also a striking absence of these changes in the solvent-exposed surfaces that form the active site or its neighboring regions.

Electrostatic calculations have successfully predicted experimental pK_a shifts in several cases (e.g., see refs. 23–25). Using DelPhi, we calculated the expected influence of the differently charged surfaces on the pK_a value of the active-site histidine. This residue is of crucial importance to both the binding of substrate and the chemical mechanism. This residue must be protonated in the enzyme/NADH binary complex before pyruvate will bind. During the chemical step, hydride from NADH is transferred to the carbonyl carbon of pyruvate and a proton from His 195 is transferred to the carbonyl oxygen to complete the formal addition of H_2 to give lactate. Hence the pK_a of His 195 in the binary enzyme/NADH complex should correlate with the observed K_M for the reduction of pyruvate by each isoenzyme. Since the crystallographic data has been acquired on the ternary complexes of enzyme/cofactor/inhibitor complexes the binary structures must be modeled to provide the framework for the electrostatic potential calculations. As the active-site loop region is disordered in every binary LDH structure determined to date, we chose to model the loop conformations by disordering them in the tetramers with a small period of high temperature molecular dynamics (see Methods and Fig. 7). Averaging the electrostatic potential calculation results over the four residues for each sequence position should give the net effect of this disorder. The results for the calculations on this model (BIN) are shown in Table V and give a Δ pK_a of 0.97 between the isoforms, in good agreement with the experimental value of 0.94 ± 0.18 (Fig. 5). Calculations on two further states derived from the crystal structures were carried out. Another, more crude, model of the binary complex was generated by discarding oxamate and the entire active-site loops (model XLOOP). Electrostatic potential calculations on this model are expected to underestimate the influence of surface charge changes on Δ pK_a, since there is no longer any shielding provided by the active-site loops. The value of Δ pK_a calculated for this model is 0.60. Next, the ternary complex itself was used for the electrostatic potential calculation (model TERN). This is expected to overestimate Δ pK_a, since the ordered active-site loop and the oxamate completely shield the active-site histidine from contact with bulk solvent, and the calculations yielded a Δ pK_a of 1.10 units. Gratifyingly, the Δ pK_a of 0.97 for the binary model (BIN) is appropriately bracketed by the expected underestimation (XLOOP) and overestimation (TERN) calculations. Hence the calculations support the notion that surface electrostatic effects underlie the altered activity response of these isoforms to the pH of their environment.

Since the electrostatic potential calculations are on a residue by residue basis they allow determination of the most influential residue positions upon Δ pK_a. This identifies mutation sites for future modulation of the kinetic properties of the isoenzymes. Such experiments could further evaluate the accuracy of these electrostatic potential calculations.

CONCLUSIONS

Although many structures of LDH from a range of species have previously been described, this study pro-

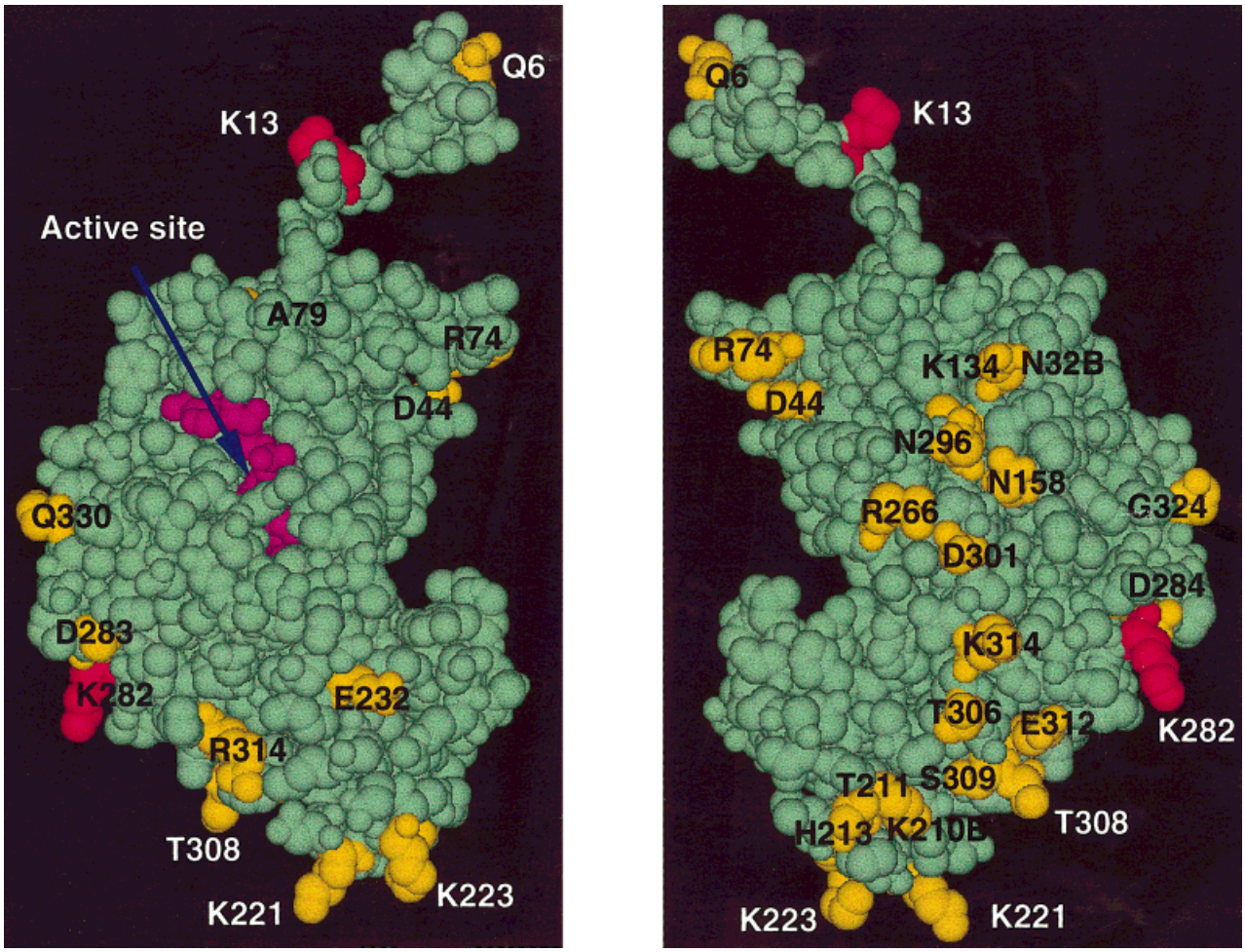

Fig. 6. Isoform variations in hLDH. Solid model representation of M-hLDH, showing amino acid side-chains of residues that differ in charge from their equivalents in H-hLDH. Residues that cause a change from either a charge to neutral or vice-versa are shown in yellow, and those that cause a change from positive to negative charge are shown in red. The NADH cofactor and oxamate substrate analogue are in purple, and all other amino acids in green. The view on the left shows the solvent-exposed face of the subunit on which the active site (labeled) is located; the view on the right shows the opposite face after a rotation of 180° around a vertical axis. In both views, the face adjoining the neighboring subunits is toward the center.

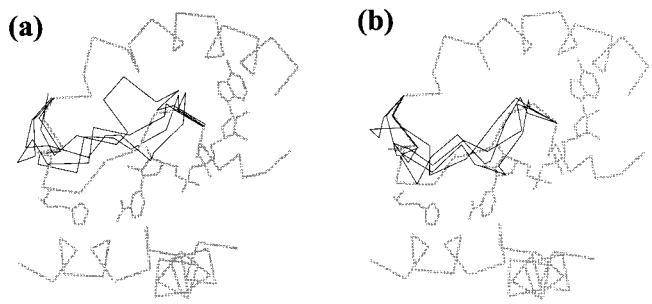

Fig. 7. Binary model. Cα positions around the active site. Heavy lines show the A subunit of the crystal structure; light lines show the active-site loops randomized by molecular dynamics. **a:** M_4-hLDH. **b:** H_4-hLDH.

vides the first crystal structures of both major human isoforms of this essential glycolytic enzyme. As these structures have been determined and refined to comparable resolutions, for the first time this study permits a legitimate comparison to be made of two isoforms with similar but clearly distinguishable kinetics. Both structures adopt subunit folds and tetrameric assemblies that are highly homologous to those described previously for other forms of LDH. The high number of independent copies of M-hLDH within the crystal asymmetric unit have allowed a comparative analysis which illustrates the relative mobility of small regions of the subunit fold, in particular the α-H C-terminal helix. Residues from this helix form direct hydrogen bonds with residues at the base of the specificity loop, a region whose closure on the occupied active-site is essential for catalysis to proceed. Nevertheless, as similar variations in the placement of this helix are noted between subunits of both H and M forms of hLDH, it seems unlikely that these movements cause the alterations in activity measured for the two isoforms. Small variations in the relative positioning of subunits within tetramers are also seen between H and M forms of hLDH. Again, however, these changes are not

TABLE V. DelPhi Calculations[†]

M isoform				H isoform			
Residue	XLOOP	BIN	TERN	Residue	XLOOP	BIN	TERN
D44	−0.6430	−1.1937	−1.3051	K6	−0.0215	−0.0397	−0.0400
D283	−0.0434	−0.0751	−0.0756	K306	−0.0276	−0.0489	−0.0530
D301	−0.1097	−0.2026	−0.2215	K308	−0.0347	−0.0623	−0.0682
E312	−0.0393	−0.0687	−0.0746	K330	−0.0171	−0.0360	−0.0360
K13	0.0281	0.0540	0.0584	R296	−0.0470	−0.0878	−0.0934
K134	0.1617	0.2898	0.3287	D81	0.0445	0.0790	0.0878
K210B	0.0485	0.0894	0.0935	D132B	0.0393	0.0747	0.0790
K221	0.0126	0.0209	0.0197	D309	0.0191	0.0304	0.0333
K223	0.0134	0.0235	0.0234	D324	0.0822	0.1030	0.1102
K282	0.0187	0.0299	0.0315	D331	0.0702	0.0946	0.1476
K304	0.0339	0.0627	0.0683	E12A	0.0214	0.0406	0.0414
R74	0.6885	1.2630	1.3938	E211	0.0525	0.0977	0.1043
R266	−0.1244	0.2291	0.2483	E282	0.0175	0.0260	0.0287
R314	0.1020	0.1776	0.1696				

[†]Entries for each model represents the Δ pK_a caused by the removal of a charged residue in the M isoform and by the addition of a charged residue in the H isoform. Hence the sums of the shifts for each model represent the calculated shift in pK_a between the M and H isoforms: XLOOP 0.60, BIN 0.97, TERN 1.10.

significant when compared to variations seen between the two separate tetramers of M_4-hLDH refined in the asymmetric unit. We note that there is strict conservation of both the identity and conformations of amino acids in the vicinity of the active sites of both enzymes. This implies that the differing kinetics of these enzymes may result from surface electrostatic effects. This is supported by a comparison of the K_M values for substrate binding to these two isoforms, where there is evidence for variation of the pK_a of the active-site histidine by about one pH unit. This alteration coincides with the expected influence of electrostatic surface charges calculated using DelPhi.

In sum, these data suggest that the two forms of hLDH have evolved to operate most efficiently in their different redox environments through simple variation of their net surface charges. A comparison of the crystal structures shows two regions in which evolutionary changes are highly constrained. First, the predominantly hydrophobic surfaces that interface with the neighboring subunits in formation of the tetramer contain minimal changes for charged side-chains between the H and M forms of hLDH. The very few changes that are tolerated in this region form salt bridges with neighboring subunit residues, hence negating any electrostatic alteration. The solvent accessible surface area of the monomer that is buried in formation of the tetramer is 5,058 Å^2, a substantial portion of the total 15,701-Å^2 surface area of a monomer. Second, the active-site region itself represents a highly evolved three-dimensional arrangement on which there must be substantial pressure for conservation. It is difficult to estimate the extent of the region over which this strong constraint is exercised, but we estimate, based on the regions in which no substantial changes occur (Fig. 6), that this region encompasses ~3,000 Å^2 of the solvent-accessible surface area. In total, these regions in which no or only conservative amino acid changes are observed between the two isoforms represent about 50% of the total monomer surface area. The remainder of the monomer surface area is available for surface charge changes that can lead to alterations in the overall molecular electrostatics, thereby influencing the kinetic parameters of the isoforms.

These studies illustrate that optimization of enzyme function in evolution can be achieved through subtle modification of amino acids remote from the active-site region itself. In human LDH, the accumulative effect of a range of surface charge changes is seen to adapt the activity of the distant active site for different environments. Changes of this kind represent a simple method for engineering enzyme activity without incurring the drastic activity changes often associated with alterations of active-site residues.

ACKNOWLEDGMENTS

The authors thank the staff at both the Daresbury SRS and EMBL Hamburg Outstation for access to synchrotron data collection facilities, as well as Oliver Donnelly for assistance with crystallization of H_4-hLDH. V.J.W. is supported by a BBSRC studentship. Coordinates and structure factors have been deposited with the Brookhaven Protein Data Base (accession numbers 1I02 and 1I10).

REFERENCES

1. Nadal-Ginard B, Markert CL. In: Markert CL, editor. Isoenzymes. Vol 2. New York: Academic Press, 1975; p 45.
2. Clarke AR, Dafforn, TR. Nicotinamide cofactor-dependent enzymes. In: Sinnott M, editor. Comprehensive biological catalysis: a mechanistic reference. Vol III. New York: Academic Press; 1998. p 1–80.
3. White JL, Hackert ML, Buehner M, Adams MJ, Ford GC Lentz PJ Smiley IE, Steindel SJ, Rossmann MG. A comparison of the structures of apo dogfish M_4-LDH and its ternary complexes. J Mol Biol 1976;102:759–779.
4. Grau UM, Trommer WE, Rossmann MG. Structure of the active ternary complex of pig heart LDH with S-lac-NAD$^+$ at 2.7 Å resolution. J Mol Biol 1981;151:289–307.
5. Dunn CR, Wilks HM, Halsall DJ, Atkinson T, Clarke AR, Muirhead H, Holbrook JJ. Design and synthesis of new enzymes based on the lactate dehydrogenase framework Philos Trans R Soc Lond 1991;332:177–184.

6. Piontek K, Chakrabarti P, Schar HP, Rossmann MG, Zuber H. Structure determination and refinement of *Bacillus stearothermophilus* lactate dehydrogenase. Proteins 1990;7:74–92.
7. Iwata S, Ohta T. Molecular basis of allosteric activation of bacterial L-lactate dehydrogenase. J Mol Biol 1993;230:21–27.
8. Dunn CR, Banfield MJ, Barker JJ, Higham CW, Moreton KM, Turgat-Balik D, Brady RL, Holbrook JJ. The structure of lactate dehydrogenase from *Plasmodium falciparum* reveals a new target for anti-malarial design. Nature Struct Biol 1996;3:912–913.
9. Dafforn TR, Badcoe IG, Sessions RB, El Hawrani AS, Holbrook JJ. Correlation of the enzyme activities of *Bacillus stearothermophilus* lacate dehydrogenase on three substrates with the results of molecular dynamics/energy minimization conformational searching. Proteins 1997;29:228–239.
10. Chapman ADM, Cortes A., Dafforn TR, Clarke AR, Brady RL. Structural basis of substrate specificity in malate dehydrogenases: crystal structure of a ternary complex of porcine cytoplasmic malate dehydrogenase, α-ketomalonate and tNAD at 2.4Å resolution. J Mol Biol 1999;285:703–712.
11. Eszes CM, Sessions RB, Clarke AR, Moreton KM, Holbrook JJ. Removal of substrate inhibition in a lactate dehydrogenase from human muscle by a single residue change. FEBS Lett 1996;399: 193–197.
12. Hewitt CO, Eszes CM, Sessions RB, Moreton KM, Dafforn TR, Takei J, Dempsey CE, Clarke AR, Holbrook JJ. A general method for relieving substrate inhibition in lactate dehydrogenases. Protein Eng 1999;12:491–496.
13. Wilks HM, Moreton KM, Halsall DJ, Hart KW, Sessions RB, Clarke AR, Holbrook JJ. Design of a specific phenyl lactate dehydrogenase by peptide loop exchange on the *Bacillus stearothermophilus* lactate dehydrogenase framework. Biochemistry 1992; 31:7802–7806.
14. Otwinoski Z, Minor W. Processing of X-ray diffraction data collected in oscillation mode. Methods Enzymol 1996;276:307–326.
15. Navaza J. AMORE—an automated package for molecular replacement. Acta Crystallogr 1994;A50:157–163.
16. Jones TA, Zou J-Y, Cowan SW, Kjeldgaard M. Improved methods for building protein structures in electron-density maps and the location of errors in these models. Acta Crystallogr [A] 1991;47: 110–119.
17. Murshidov GN, Vagin AA, Dodson EJ. Refinement of macromolecular structures by the maximum-likelihood method. Acta Crystallogr [D] 1997;53:240–255.
18. Lamzin VS, Wilson KS. Automated refinement of protein models. Acta Crystallogr [D] 1993; 49:129–147.
19. Leatherbarrow RJ. Grafit 3.0. Staines, UK: Erithracus Software, 1992.
20. Gilson MK, Honig BK. Calculation of electrostatic potentials in an enzyme active site. Nature 1987;330:84–86.
21. Nishiyama M, Kinoshita M, Kudo H, Horinouchi S, Tanokura M. Enhancement of the turnover number of thermostable malate dehydrogenase by deleting hydrogen bonds around the catalytic site. Biochem Biophys Res Commun 1996;225:844–848.
22. El Hawrani, AS, Moreton KM, Sessions RB, Clarke AR, Hobrook JJ. Engineering surface loops of proteins—a preferred strategy for obtaining new enzyme function. Trends Biotechnol 1994;12:207–211.
23. Nielsen JE, Andersen KV, Honig B, Hooft RWW, Klebe G, Vriend G, Wade RC. Improving macromolecular electrostatics calculations. Protein Eng 1999;12:657–662.
24. Tishmack PA, Bashford D, Harms E, VanEtten RL. Use of H-1 NMR spectroscopy and computer simulations to analyze histidine p*K* (a) changes in a protein tyrosine phosphatase: experimental and theoretical determination of electrostatic properties in a small protein. Biochemistry 1997;36:11984–11994.
25. Antosiewicz J, McCammon JA, Gilson MK. Prediction of pH-dependent properties of proteins. J Mol Biol 1994;238:415–436.
26. Criddle RS, McMurray CH, Gutfreund H. Factors controlling the interconversion of enzyme–substrate compounds of pig heart lactate dehydrogenase. Nature 1968;220:1091–1095.
27. Boland MJ, Gutfreund H. Binding of pyruvate and the interconversion of pyruvate-containing ternary complexes. Biochem J 1975; 151:715–727.
28. Stinson RA, Holbrook JJ. Equilibrium binding of nicotinamide nucleotides to lactate dehydrogenases. Biochem J 1973;131:719–728.
29. Whitaker JR, Yates DW, Bennett NG, Holbrook JJ, Gutfreund H. The identification of intermediates in the reaction of pig heart lactate dehydrogenase and its substrates. Biochem J 1974;139:677–697.
30. Bennett NG, Gutfreund H. The kinetics of the interconversion of intermediates of the reaction of pig muscle lactate dehydrogenase with oxidized nicotinamide-adenine dinucleotide and lactate. Biochem J 1973;135:81–85.